Calcium-triggered fusion of lipid membranes is enabled by amphiphilic nanoparticles

Mukarram A. Tahir[a], Zekiye P. Guven[b], Laura R. Arriaga[c,1], Berta Tinao[c], Yu-Sang Sabrina Yang[d], Ahmet Bekdemir[b], Jacob T. Martin[d], Alisha N. Bhanji[a], Darrell Irvine[a,d], Francesco Stellacci[b], and Alfredo Alexander-Katz[a,1]

[a]Department of Materials Science and Engineering, Massachusetts Institute of Technology, Cambridge, MA 02142; [b]Institute of Materials, Ecole Polytechnique Federale de Lausanne, 1015 Lausanne, Switzerland; [c]Department of Theoretical Condensed Matter Physics, Autonoma University of Madrid, 28049 Madrid, Spain; and [d]Koch Institute for Integrative Cancer Research, Massachusetts Institute of Technology, Cambridge, MA 02139

Edited by Monica Olvera de la Cruz, Northwestern University, Evanston, IL, and approved June 20, 2020 (received for review March 13, 2019)

Lipid membrane fusion is an essential process for a number of critical biological functions. The overall process is thermodynamically favorable but faces multiple kinetic barriers along the way. Inspired by nature's engineered proteins such as SNAP receptor [soluble N-ethylmale-imide-sensitive factor-attachment protein receptor (SNARE)] complexes or viral fusogenic proteins that actively promote the development of membrane proximity, nucleation of a stalk, and triggered expansion of the fusion pore, here we introduce a synthetic fusogen that can modulate membrane fusion and equivalently prime lipid membranes for calcium-triggered fusion. Our fusogen consists of a gold nanoparticle functionalized with an amphiphilic monolayer of alkanethiol ligands that had previously been shown to fuse with lipid bilayers. While previous efforts to develop synthetic fusogens have only replicated the initial steps of the fusion cascade, we use molecular simulations and complementary experimental techniques to demonstrate that these nanoparticles can induce the formation of a lipid stalk and also drive its expansion into a fusion pore upon the addition of excess calcium. These results have important implications in general understanding of stimuli-triggered fusion and the development of synthetic fusogens for biomedical applications.

membrane fusion | nanoparticles | proteins | drug delivery

Lipid membrane fusion is an essential component of fundamental cellular processes like cargo transport, pathogenic interactions, reproduction, morphogenesis, and communication (1–6). Multiple transient intermediates with associated energy barriers, however, precede the fusion of membranes (7–10). The fusion process requires close proximity between the membranes, which creates repulsive hydration forces between polar head groups of the proximal leaflets (11). Acyl chains of lipids from the apposed membranes must develop contact in the intervening solvent, resulting in the formation of a stalk between the proximal leaflets that may facilitate lipid exchange between the membranes (12, 13). Expansion of this fusion stalk is then necessary to drive distal leaflet contact, which may result in a metastable hemifusion intermediate or direct formation of a fusion pore (8, 14). In biological systems, this sequence of events is directed by an ensemble of fusion proteins, with the effective pathway being specific to the underlying process that the fusion process enables (15). An interesting example is synaptic vesicle fusion, which happens at the junction of two neurons where neurotransmitters are exchanged, because it is fast and synchronized with the release of calcium upon the arrival of an action potential (16). The process is driven by a complementary set of SNAP receptor (SNARE) proteins that are present in both the neurotransmitter vesicles and the plasma membranes and form a tight complex that drives the membranes into close proximity and also generates perturbations that promote the nucleation of a fusion stalk between the proximal leaflets. Once calcium ions are introduced from nearby ion channels, the stalk rapidly expands and ruptures into a fusion pore, causing exocytotic release of neurotransmitters (17, 18).

Inspired by this neural machinery, here we introduce a synthetic fusogen that is analogously capable of performing calcium-triggered fusion. In particular, the fusogen consists of an amphiphilic nanoparticle composed of a gold core functionalized with a mixed monolayer of alkanethiol ligands. Such nanoparticles had been shown to induce protein-mimetic perturbations in surrounding lipids (19), with their ability to promote the incidence of lipid tail protrusions bearing striking resemblance to similar effects hypothesized to underlie the function of membrane-bound fusion peptides (20). There is prior evidence that the nucleation of a fusion stalk between closely apposed lipid bilayers requires acyl chains from the proximal leaflets to protrude and intercalate in the intervening solvent (21). This creates a hydrophobic channel that connects both bilayers. If nanoparticles can similarly facilitate the creation of this channel by bridging the hydrophobic regions of both bilayers, which is plausible given their ability to fuse with such bilayers (22, 23), they may be able to function as synthetic bridges or fusogens and mediate fusion between lipid membranes. To probe this possibility, we modeled the interaction of planar 1,2-dioleoyl-sn-glycero-3-phosphocholine (DOPC) lipid bilayers separated by a solvent layer of 10 water molecules per inner lipid through coarse-grained molecular dynamics simulations (*Methods*). This corresponds to an interbilayer head-group separation of ∼1 nm and is commensurate with the critical distance for spontaneous stalk formation between protein-free lipid membranes as measured in

Significance

Lipid membrane fusion is a critical component of biological transport, communication, and developmental processes. The fusion reaction is kinetically constrained since it contains multiple large energy barriers, so proteins and ions are used by natural systems to intervene and catalyze the reaction toward biologically relevant timescales. Here, we demonstrate how amphiphilic nanoparticles can prime lipid membranes for fusion so that complete fusion proceeds only upon exposure to an excess of calcium or other stimulus that would stress the outer leaflet. This is a major advance in the nascent field of controlled fusion and may unlock new avenues of research on how nanomaterials can be designed from first principles to perform targeted functional roles in biological systems.

Author contributions: M.A.T., L.R.A., D.I., F.S., and A.A.-K. designed research; M.A.T., Z.P.G., L.R.A., B.T., Y.-S.S.Y., J.T.M., A.N.B., and A.A.-K. performed research; M.A.T., Z.P.G., L.R.A., B.T., Y.-S.S.Y., A.B., and J.T.M. contributed new reagents/analytic tools; M.A.T., Z.P.G., L.R.A., B.T., Y.-S.S.Y., A.N.B., and A.A.-K. analyzed data; and M.A.T., L.R.A., D.I., F.S., and A.A.-K. wrote the paper.

The authors declare no competing interest.

This article is a PNAS Direct Submission.

[1]To whom correspondence may be addressed. Email: lrarriaga@quim.ucm.es or aalexand@mit.edu.

This article contains supporting information online at https://www.pnas.org/lookup/suppl/doi:10.1073/pnas.1902597117/-/DCSupplemental.

First published July 20, 2020.

prior work (24). With propensity for fusion of lipid bilayers being correlated with curvature (25), this system additionally represents an upper bound to the fusion barrier and is, therefore, a stringent test of a synthetic agent's fusogenic ability. As a first approximation, we assume that the nanoparticle has fully embedded into one of the membranes through an insertion pathway that has previously been extensively characterized (22, 26, 27), and that the interacting membranes are already in close proximity. Such conditions can be relaxed, but the results do not change significantly, as we later see in the case of nanoparticle-mediated interaction between lipid vesicles. We probe this system in the presence of a 2-nm gold nanoparticle functionalized with a 1:1 mixture of 11-mercapto-1-undecanesulphonate (MUS) and 1-octanethiol (OT), as shown in Fig. 1 *A* and *B*. Clearly, the nanoparticle initiates a stable state of lipid exchange between the proximal leaflets, as shown in Fig. 1*C*, after a latent state that persists on a microsecond timescale. Note that this timescale is a lower bound and is likely orders of magnitude higher in experiments where nanoparticle and lipid membranes are present at much lower concentrations. The end state is a stalk-like structure between the proximal leaflets, where the nanoparticle partitions charged ligand end groups to the periphery and has hydrophobic ligands freely associating with the hydrophobic core of the stalk.

The incidence of stalk formation on this timescale is anomalous because, owing to the requirement of hydrophobic contact between a pair statistically independent lipid tail protrusions (21), planar lipid membranes are typically not observed to fuse on biologically relevant timescales in the absence of a fusogenic agent. The ability of membrane-embedded nanoparticles to drive lipid mixing under these circumstances is therefore an intriguing result that merits further investigation. As shown in Fig. 1*D*, a time series of hydrophobic contacts between the nanoparticle and the adjacent bilayer's lipids and between lipids from the two bilayers reveals that the formation of the stalk is initiated by hydrophobic contact between the nanoparticle's exposed surface monolayer and a lipid from the adjacent bilayer. Subsequent persistence of nanoparticle-lipid contact and a continuous increase in lipid-lipid hydrophobic contacts indicate that the nanoparticle functions as a bridge over which lipids can be exchanged between proximal leaflets. The overall behavior is consistent with the *cis* lipid

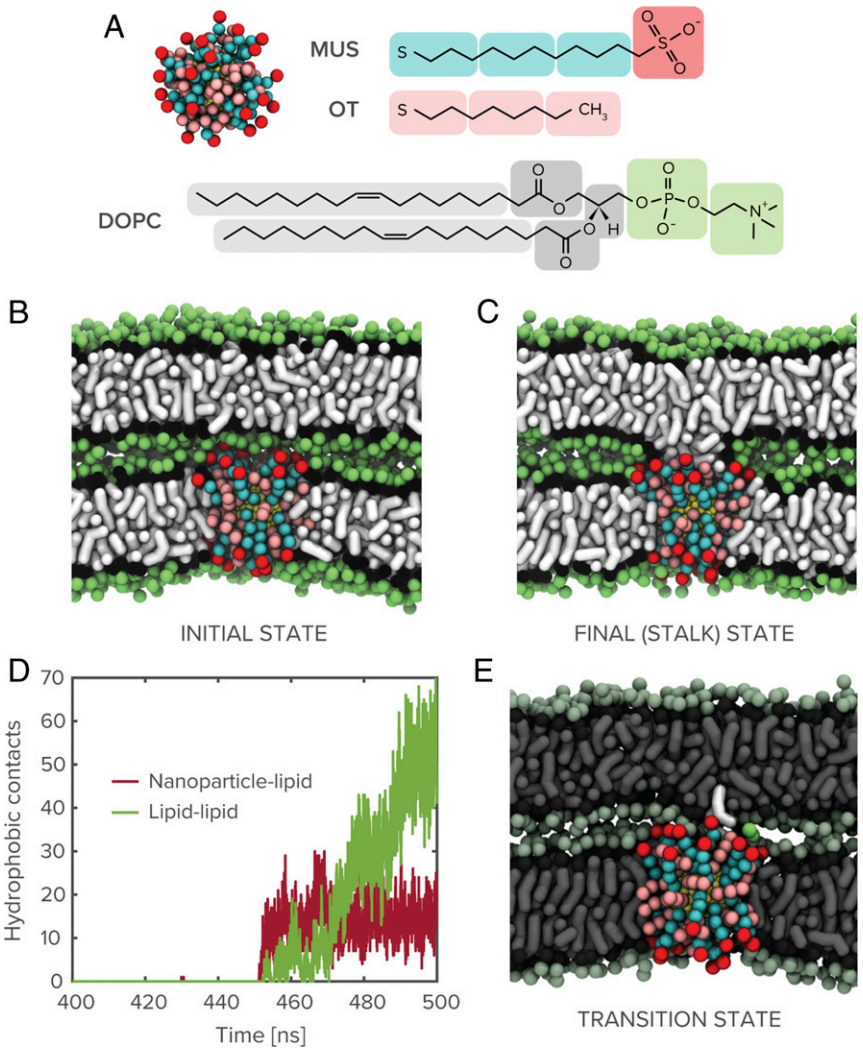

Fig. 1. System components and nanoparticle-mediated stalk formation. (*A*) Coarse-grained representation of the amphiphilic MUS:OT nanoparticles studied in molecular dynamics simulations shown alongside chemical structure of the nanoparticle surface ligands and a DOPC lipid molecule. (*B* and *C*) Snapshots of initial simulation state and nanoparticle-induced stalk between dehydrated lipid membranes (water molecules not shown for clarity). (*D*) Time series plot of hydrophobic (alkyl-alkyl) contacts between nanoparticle and lipids from apposed bilayer and between lipids from the two bilayers. (*E*) Transition state for nanoparticle-mediated stalk formation, identified through committor analysis of the 2-nm MUS:OT trajectory, involves the extraction of a lipid from the adjacent bilayer toward the membrane-embedded nanoparticle.

mixing that is characteristic of stalk formation between lipid vesicles as observed in previous work (2).

To identify the origin of this effect, we performed committor analysis on the simulation trajectories to identify the transition state for nanoparticle-mediated stalk formation between lipid membranes. Briefly, this process involves extracting a subset of the simulation trajectory surrounding the critical event, launching a series of independent simulations with randomized velocities, and determining the fraction that proceed to stalk formation to determine a transition probability (see *Methods* for further details). As shown in Fig. 1*E*, the transition state (corresponding to the state with transition probability of 0.5) between sonly surface attraction and stalk formation occurs with the nanoparticle extracting a single lipid from the adjacent bilayer into its surface monolayer. Following this commitment, subsequent lipid exchange between the inner bilayer leaflets is spontaneous and bridged by the initial nanoparticle–lipid complex. The ability of the nanoparticle to perform lipid extraction on a microsecond timescale is itself intriguing, given the high energetic penalty associated with such an extraction under ordinary circumstances (28). As shown in the plot of the interaction energy between the extracted lipid and system components (*SI Appendix*), however, this energetic penalty is substantially compensated by significant compatibility between the extracted lipid and the amphiphilic character of the nanoparticle's exposed surface monolayer.

While the above simulations demonstrate a mechanism through which nanoparticles may support stalk formation between lipid membranes, the preexistence of a dehydrated interface and extreme absence of curvature preclude an understanding of the broader mechanism through which nanoparticles may fully modulate the fusion of lipid-bound compartments. To uncover the full pathway for nanoparticle-mediated fusion of small unilamellar vesicles

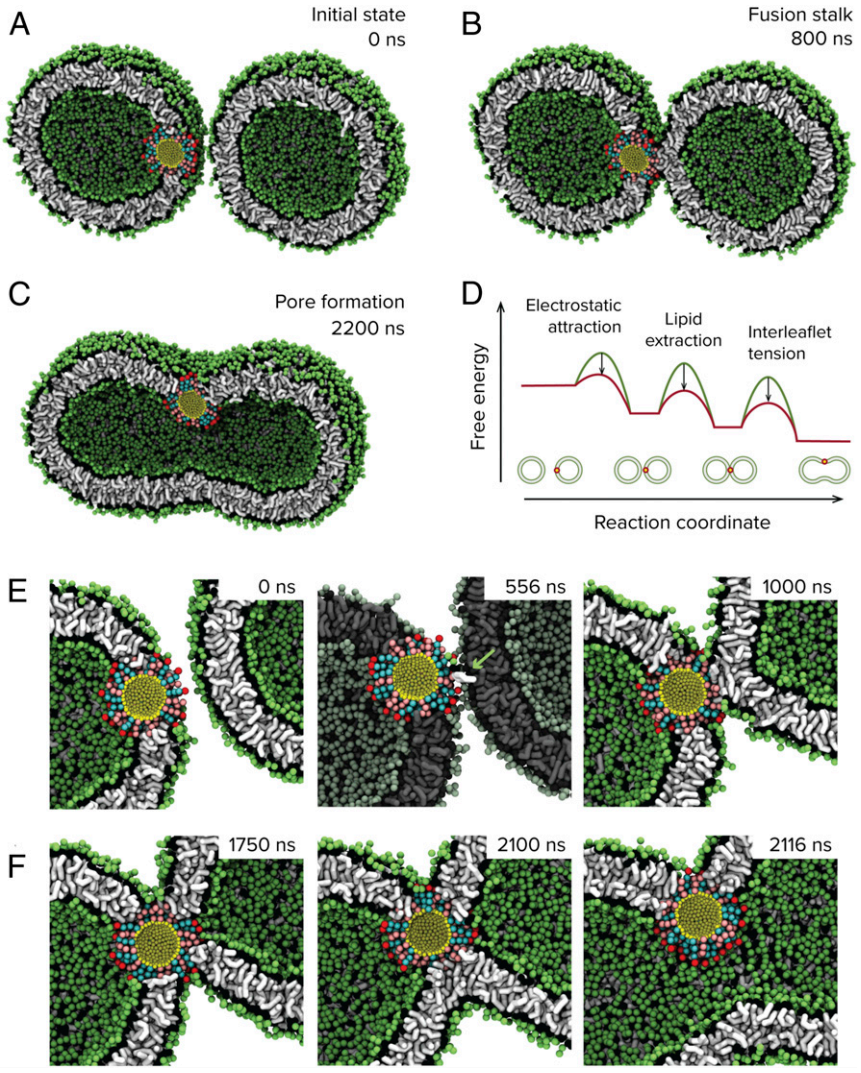

Fig. 2. Molecular dynamics simulation of nanoparticle-driven vesicle fusion. Coarse-grained molecular dynamics simulations reveal a mechanism through which nanoparticles can drive fusion between lipid membranes. (*A* and *B*) The presence of membrane-embedded nanoparticles drives the vesicles into close proximity, which, in turn, facilitates the ability of the nanoparticle to extract lipids from the adjacent bilayer and nucleate the formation of a fusion stalk between the membranes. (*C*) Subsequent influx of Ca^{2+} results in mechanical tension between the inner and outer leaflets of this complex, modeled here by removal of a subset of lipids from the outer leaflets at 1,000 ns, and causes expansion of the stalk into a fusion pore. (*D*) Proposed pathway summarizing how the nanoparticle reduces key free energy barriers during membrane fusion. The free energy profiles are schematic and not to scale. (*E*) The transition to stalk proceeds through a lipid extraction pathway similar to that observed for nanoparticle-mediated stalk formation between planar lipid membranes. The extracted lipid is in white and highlighted with an arrow. (*F*) Expansion of the fusion stalk upon condensation of outer area-per-lipid requires reorganization of the nanoparticle ligands in a manner that permits contact between inner leaflets of the two vesicles.

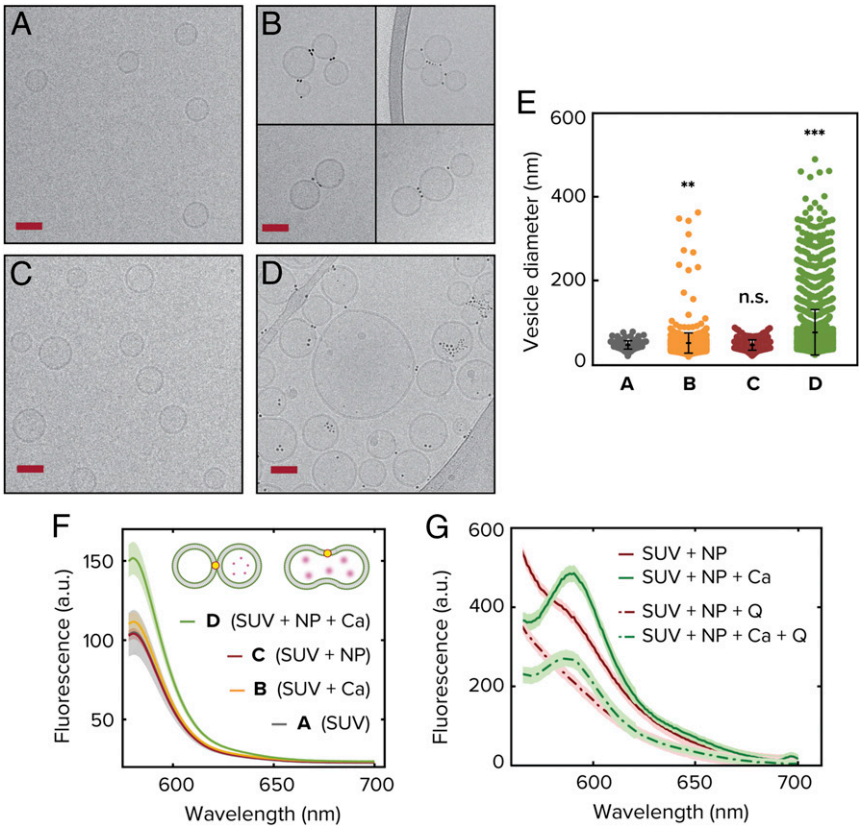

Fig. 3. Experimental realization of vesicle fusion driven by amphiphilic nanoparticles. Cryogenic electron microscopy images are shown on the left for: unilamellar DOPC vesicles as synthesized (*A*), vesicles upon addition of $CaCl_2$ in absence of nanoparticles (*B*), vesicles upon addition of 3-nm MUS:OT gold nanoparticles (*C*), and vesicles upon influx of $CaCl_2$ following incubation with nanoparticles (*D*). (Scale bars, 50 nm.) (*E*) Vesicle size distribution as measured from quantitative analysis of the microscopy images. Each colored point corresponds to a different vesicle and in total the analysis was done over more than 4,000 SUVs. The error bars correspond to the SD and is centered around the mean of the distribution. (*F*) Fluorescence emission spectra from the sulforhodamine B content mixing assay. As the dye gets diluted by fusion with empty vesicle, the signal increases (see text for details). (*G*) FRET assay indicating full fusion for the case in which $CaCl_2$ is added to a system already incubated with NPs. The signal is clearly seen at 582 nm and does not disappear when quencher Q is added, indicating inner-leaflet mixing. The excitation wavelength is 463 nm. In the absence of $CaCl_2$, the FRET signal disappears upon the addition of Q implying lipid mixing only in the outer leaflets.

(SUVs), we performed unbiased molecular dynamics simulations of 20-nm DOPC liposomes. These SUVs are initially separated by a minimum distance of 2 nm. In the absence of an embedded nanoparticle, the vesicles show no attractive interactions or fusion events over multiple microseconds. When a 3-nm MUS:OT nanoparticle is introduced into one of the vesicles as shown in Fig. 2*A*, there is a pronounced increase in the ability of the vesicles to maintain their initial proximity, owing to electrostatic attraction between exposed sulfonate groups of the embedded nanoparticle and lipid head groups from the neighboring vesicle. The resulting dehydrated interface bears similarities to the planar systems studied above and, predictably, we observe nanoparticle-mediated stalk formation between the vesicles (Fig. 2 *B* and *E*). The typical timescale to stalk formation we find in simulations is around 1 μs, but this might be just due to the fact that we are working at extremely high SUV concentrations. We allowed these simulations to proceed for multiple microseconds and observed minimal change in the structure of this complex. To probe if there would be any difference if the nanoparticles are not embedded in the membrane completely, we ran simulations with a free nanoparticle in the solvent region and allowed the system to evolve under no constraints. As shown in *SI Appendix*, Fig. S11, we find that this system also proceeds to stalk formation, with the resulting formation more closely resembling those observed in experiments on SUVs and visualized using cryogenic transmission electron microscopy (TEM) (discussed below). The system being arrested at the stalk state is not surprising since further expansion of the stalk requires the development of *trans*-leaflet contact, which the nanoparticle is unable to drive because it is in a conformation that does not permit it to assert point-like forces to this effect, whereas for SNARE transmembrane domains are believed to be able to do so (29, 30). Expansion of the fusion stalk into a fusion pore in our case would therefore be entirely dependent on the effects of an external stimulus. Previous insightful studies from Grubmuller and coworkers have shown that mechanical stress due to the condensation of the area-per-lipid in the outer leaflet leading to membrane asymmetry can drive complete fusion in a similar system (7). An avenue to achieve this asymmetry is to have an excess of Ca^{2+} in the outer solvent, which has been shown by SAXS to drive electrostatic condensation of the area-per-lipid of 1,2-dipalmitoyl-sn-glycero-3-phosphocholine (DPPC) lipids (31), with maximal condensation of ∼9% obtained at an excess of 2 mM Ca^{2+}. We note that in this study the lipids were in their liquid state. To probe this effect, we analogously introduce membrane asymmetry in our simulations, by deletion of 9% of *cis* (outer) leaflet lipids (*Methods*), and indeed observed spontaneous expansion of the connecting stalk into a fusion pore that subsequently enabled content mixing between the vesicles (Fig. 2 *C* and *F*). This process appears to be stochastic in nature, and within the simulation timescale of 10 μs per trajectory we observed five of seven replicas proceed to full fusion.

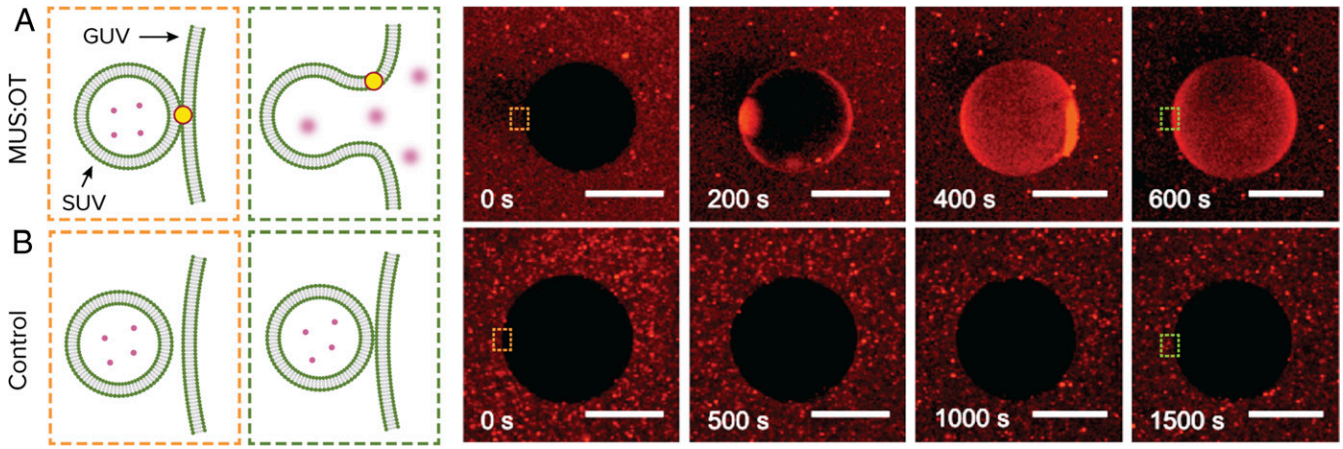

Fig. 4. Macroscale demonstration of nanoparticle-mediated fusion. Sulforhodamine B encapsulated in small liposomes (SUVs) is released into GUVs, upon influx of Ca^{2+}, only if the system is incubated with amphiphilic nanoparticles. (*A*) Time sequence of confocal fluorescence images showing fusion of liposomes with GUVs in the presence of nanoparticles. (*B*) Time sequence of confocal fluorescence images showing that fusion does not occur in the absence of nanoparticles. Time 0 represents a snapshot right before the addition of Ca^{2+}. Note that the timescale of fusion in this case is limited by the diffusion of calcium toward the fusion sites. (Scale bars, 50 μm.)

In order to test the simulation results experimentally and confirm different parts of the uncovered pathway, we used several complementary techniques. First, we used cryo-electron microscopy to directly probe the ability of amphiphilic nanoparticles to modulate interactions between lipid vesicles in an experimental setting. We formed small unilamellar DOPC vesicles (SUVs) with an average diameter of 50 nm through repeated extrusion of a lipid suspension prepared using the film rehydration technique (*Methods*). A representative image of the resulting vesicle population is shown in Fig. 3*A*. As a control for testing what is the effect of purely stressing the membranes without NPs, we added $CaCl_2$ at a concentration of 2 mM to the system. This concentration of $CaCl_2$ has been shown to roughly correspond to a maximal condensation of area-per-lipid for this particular head group, as explained above (31). As shown in Fig. 3*B*, minimal fusion of the vesicles is observed. As shown in Fig. 3*C*, in the absence of $CaCl_2$ but with the addition of MUS:OT NPs of average diameter of 2.4 nm and incubation for 60 min results in significant clustering of the vesicles, with the nanoparticles appearing to bridge membranes in a similar manner to the simulations (Fig. 2*E* and *SI Appendix*, Fig. S11). This can be clearly seen if one examines the edge of the outer leaflet in the area where the nanoparticles are present (*SI Appendix*, Fig. S12). As mentioned above, to induce interleaflet tension we change the area per lipid in the outer membrane by introducing 2 mM $CaCl_2$ into the system. We observe a large increase in the average diameter of the vesicles that is indicative of fusion events throughout the sample (Fig. 3 *D* and *E*). In Fig. 3*E*, we observe that the diameter of vesicles increases markedly upon the addition of $CaCl_2$ only if the solution is first incubated with nanoparticles. We studied >4,000 SUVs to obtain the statistics shown in Fig. 3*E*, where each colored point corresponds to a different counted vesicle. Note the large number of outliers toward large sizes in the NP + Ca^{2+} system. The minimum total efficiency of fusion is represented by the number of vesicles bigger than the average control size. In our case we find that 81% of the vesicles are larger than the control average size.

To further probe this system, we used fluorescence assays to directly test content mixing and lipid mixing in both leaflets. In Fig. 3*F*, we show the results for content mixing, where we probed this system using a sulforhodamine B content mixing assay (*Methods*). Content mixing will be expected if empty SUVs fuse with SUVs containing sulforhodamine B just above the self-quenching concentration. Commensurate with simulation and microscopy results, we observe a significant uptick in the emission signal indicating content mixing only upon influx of calcium if the vesicles are previously incubated with the MUS:OT nanoparticles. Previous experiments have shown using Förster resonance energy transfer (FRET) that amphiphilic nanoparticles can induce lipid mixing, but not content mixing (32), further underscoring the necessity of calcium in driving the system from "frozen-stalk" to full fusion. To further probe if this system undergoes full fusion upon calcium stimulation, we perform a lipid mixing assay to probe lipid mixing in the inner leaflet only. To do this, we use two populations of DOPC SUV containing different lipid dyes that serve as a FRET pair as was done previously (see *Methods* for details). However, this time we add a fluorescence quencher to the external medium. If mixing occurs only in the outer leaflet, the FRET signal can be quenched, while if the inner leaflets mix, we should still observe a FRET signal. Our results shown in Fig. 3*G* indicate that a 1:1 mixture of the different vesicles containing each one of the FRET lipid-bound dyes incubated with NPs under the same conditions as those used for content mixing indeed undergo full fusion upon 2 mM $CaCl_2$ addition. This can be seen by the fact that the peak at 582 nm, which is the emission wavelength of the receptor dye, does not disappear even with the addition of the quencher Q (lowest dashed curve). In the absence of calcium, however, we observe a weak mixing signal that gets suppressed once we add the quencher (upper continuous and dashed lines). The experiments in the current work thus provide direct evidence that amphiphilic nanoparticles can prime lipid vesicles for fusion and, upon the arrival of calcium, drive pore expansion and full fusion.

To see if this effect could potentially work on a larger scale, we formed giant unilamellar DOPC vesicles (GUVs) and characterized their interaction using confocal optical microscopy. SUVs containing sulforhodamine B at self-quenching concentration were first incubated in a mixture with GUVs and with MUS:OT nanoparticles for 60 min. As shown in Fig. 4*A* and Movie S4, introduction of calcium at 20 mM following incubation results in fusion, as indicated by the increase in fluorescent intensity of the GUV interior. We used a higher concentration compared to the SUV experiments because calcium is inserted locally using a pipette and mixing is slow as we do not stir the suspension. As a control, we also add calcium in the same way to the mixture of GUVs and SUVs without MUS:OT nanoparticles. As shown in Fig. 4*B* and Movie S5, we do not see a distinct increase in GUV fluorescent content following the introduction of calcium in this case.

To further analyze this SUV + GUV system in a similar fashion to the case of pure SUVs, we also conducted FRET

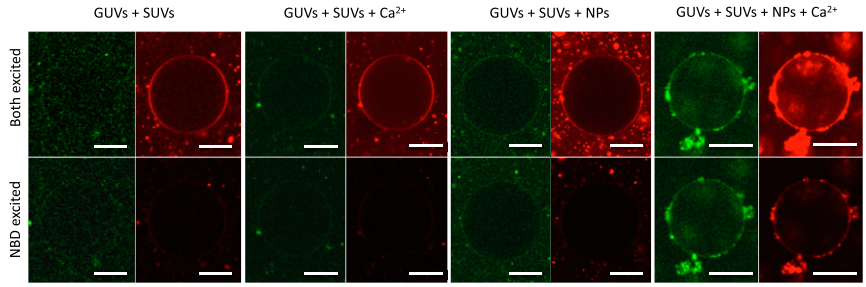

Fig. 5. Simultaneous lipid and content mixing assay of small unilamellar vesicles (SUV) and giant unilamellar vesicles (GUV). Confocal microscopy images of GUVs labeled with Rh-1,2-di-(9Z-octadecenoyl)-sn-glycero-3-phosphoethanolamine (DOPE) (red) and large unilamellar vesicles (LUV) labeled with NBD-DOPE (green) containing sulforhodamine at self-quenching concentration. In *Upper*, we use two different lasers with wavelength corresponding to the excitation wavelength of NBD and Rho to excite the different fluorophores. In contrast, in *Lower*, only the excitation wavelength of NBD is used to obtain FRET. Each collection of four images is a different GUV representative of the situation indicated in the labels after 20 min of incubation. (Scale bars, 10 μm.)

experiments with a pair of lipid dyes consisting of Sulforhodamine B-labeled lipids and NBD-labeled lipids to directly observe lipid mixing. We also incorporated free Sulforhodamine B at self-quenching concentrations in the interior of the SUVs to probe content mixing simultaneously, in a manner that is similar to previous experiments (33, 34). In Fig. 5, we show the evolution of a vesicle after 20 min of incubation in each successive state (*Methods*). Clearly, in the presence of NPs alone the FRET signal is present, particularly for the small vesicles outside the large GUV in the center. As mentioned above, previous studies from our groups had already demonstrated lipid mixing using a more sensitive FRET assay for this system and found maximal mixing at ∼2 h (32), which corresponds to a longer time scale than the one studied here. However, upon the addition of calcium, we see rapid mixing (within seconds) in a large population of GUVs, indicating a large number of lipids labeled with NBD have been added to the membrane of the GUVs (*SI Appendix*, Fig. S13), further corroborating the fusion hypothesis. In Fig. 5, *Right*, it is also evident that the interior of the vesicle is more fluorescent than the background, indicating content mixing and not leakage as responsible for the increase in fluorescence in the interior of the GUV. We must note that while our work shows unequivocally that our synthetic fusogens promote SUV docking and lipid exchange, and can serve for controlling fusion even with larger GUVs, further work in this area is needed to find the optimal conditions to control the fusion cascade in GUVs.

In conclusion, we have introduced a synthetic nanoparticle fusogen that can mediate fusion between lipid membranes and be controlled using an external stimulus. The pathway through which this occurs demonstrates that amphiphilic nanoparticles facilitate fusion through the reduction of key energy barriers associated with development of initial membrane proximity and stalk formation somewhat resembling its natural counterparts. In particular, the embedded nanoparticle exposes excess anionic sulfonate groups that demonstrate attractive interactions with polar head groups of the opposing bilayer and counteract the repulsive hydration forces that would otherwise inhibit close approach of the membranes. The amphiphilic character of this exposed monolayer also reduces the energy barrier associated with extraction of a lipid from the opposing membrane, resulting in spontaneous hydrophobic contact and nucleation of a fusion stalk between the membranes on a microsecond timescale. With these principal energy barriers to fusion overcome by the action of the embedded nanoparticle, the introduction of calcium condenses the *cis* leaflet's area-per-lipid, creating a mechanical asymmetry between the membranes leaflets that ultimately drives *trans* leaflet contact and rapidly expands the stalk into a fusion pore. Our results thus uncover an area of designing protein-inspired nanostructures from first principles using monolayer-protected nanoparticles and can be useful in understanding biological vesicle fusion as well as enabling new technological innovations in this area.

Materials and Methods

Molecular dynamics simulations were performed using the Gromacs package and system constituents modeled using the Martini force field. Committor analysis was used for determining the transition state for nanoparticle-mediated fusion between lipid membranes. Nanoparticles were synthesized using the Brust method, and interaction with lipid vesicles was imaged using cryogenic electron microscopy. Lipid and content mixing assays were utilized for quantifying interactions between lipid vesicles that are mediated by the presence of nanoparticles. See *SI Appendix* for further details.

Data Availability Statement. Molecular dynamics simulation states (model for nanoparticles, nanoparticle-mediated fusion planar membranes, and nanoparticle-mediated fusion of vesicles) and experimental data (TEM snapshots and raw experimental measurements) have been deposited to FigShare (https://figshare.com/collections/Calcium-triggered_fusion_of_lipid_membranes_is_enabled_by_amphiphilic_nanoparticles/5023487/1).

ACKNOWLEDGMENTS. M.A.T. acknowledges support from the US Department of Energy through the Computational Science Graduate Fellowship under Contract DE-FG02-97ER25308. Molecular dynamics simulations were performed in the Extreme Science and Engineering Discovery Environment and supported by the National Science Foundation under Contract TG-DMR130042. This work was supported in part by the US Army Research Laboratory and the US Army Research Office through the Institute for Soldier Nanotechnologies under Contract W911NF-13-D-0001. Z.P.G. acknowledges support from the Swiss National Science Foundation and the NCCR Molecular Systems Engineering. L.R.A. acknowledges financial support from Ramón y Cajal Program Grant RYC2018-025575-I and "Retos Investigación" Program Grant RTI2018-101953-A-I00) from the Spanish Ministry of Science, Innovation, and Universities.

1. Y. A. Chen, R. H. Scheller, SNARE-mediated membrane fusion. *Nat. Rev. Mol. Cell Biol.* **2**, 98–106 (2001).
2. J. Diao *et al.*, A single-vesicle content mixing assay for SNARE-mediated membrane fusion. *Nat. Commun.* **1**, 54 (2010).
3. R. Jahn, T. C. Südhof, Membrane fusion and exocytosis. *Annu. Rev. Biochem.* **68**, 863–911 (1999).
4. S. C. Harrison, Viral membrane fusion. *Nat. Struct. Mol. Biol.* **15**, 690–698 (2008).
5. T. C. Südhof, J. E. Rothman, Membrane fusion: Grappling with SNARE and SM proteins. *Science* **323**, 474–477 (2009).
6. T. Söllner, J. E. Rothman, Neurotransmission: Harnessing fusion machinery at the synapse. *Trends Neurosci.* **17**, 344–348 (1994).
7. H. J. Risselada, G. Bubnis, H. Grubmüller, Expansion of the fusion stalk and its implication for biological membrane fusion. *Proc. Natl. Acad. Sci. U.S.A.* **111**, 11043–11048 (2014).
8. V. S. Malinin, B. R. Lentz, Energetics of vesicle fusion intermediates: Comparison of calculations with observed effects of osmotic and curvature stresses. *Biophys. J.* **86**, 2951–2964 (2004).
9. L. V. Chernomordik, M. M. Kozlov, Mechanics of membrane fusion. *Nat. Struct. Mol. Biol.* **15**, 675–683 (2008).
10. A. Grafmüller, J. Shillcock, R. Lipowsky, The fusion of membranes and vesicles: Pathway and energy barriers from dissipative particle dynamics. *Biophys. J.* **96**, 2658–2675 (2009).
11. E. Schneck, F. Sedlmeier, R. R. Netz, Hydration repulsion between biomembranes results from an interplay of dehydration and depolarization. *Proc. Natl. Acad. Sci. U.S.A.* **109**, 14405–14409 (2012).
12. A. Efrat, L. V. Chernomordik, M. M. Kozlov, Point-like protrusion as a prestalk intermediate in membrane fusion pathway. *Biophys. J.* **92**, L61–L63 (2007).

13. Y. Kozlovsky, M. M. Kozlov, Stalk model of membrane fusion: Solution of energy crisis. *Biophys. J.* **82**, 882–895 (2002).
14. H. Chakraborty, P. K. Tarafdar, M. J. Bruno, T. Sengupta, B. R. Lentz, Activation thermodynamics of poly(ethylene glycol)-mediated model membrane fusion support mechanistic models of stalk and pore formation. *Biophys. J.* **102**, 2751–2760 (2012).
15. L. V. Chernomordik, M. M. Kozlov, Protein-lipid interplay in fusion and fission of biological membranes. *Annu. Rev. Biochem.* **72**, 175–207 (2003).
16. A. T. Brunger, U. B. Choi, Y. Lai, J. Leitz, Q. Zhou, Molecular mechanisms of fast neurotransmitter release. *Annu. Rev. Biophys.* **47**, 469–497 (2018).
17. J. Diao *et al*., Synaptic proteins promote calcium-triggered fast transition from point contact to full fusion. *elife* **1**, e00109 (2012).
18. J. B. Sørensen, Conflicting views on the membrane fusion machinery and the fusion pore. *Annu. Rev. Cell Dev. Biol.* **25**, 513–537 (2009).
19. R. C. Van Lehn, A. Alexander-Katz, Membrane-embedded nanoparticles induce lipid rearrangements similar to those exhibited by biological membrane proteins. *J. Phys. Chem. B* **118**, 12586–12598 (2014).
20. P. Larsson, P. M. Kasson, Lipid tail protrusion in simulations predicts fusogenic activity of influenza fusion peptide mutants and conformational models. *PLOS Comput. Biol.* **9**, e1002950 (2013).
21. P. M. Kasson, E. Lindahl, V. S. Pande, Atomic-resolution simulations predict a transition state for vesicle fusion defined by contact of a few lipid tails. *PLOS Comput. Biol.* **6**, e1000829 (2010).
22. R. C. Van Lehn *et al*., Lipid tail protrusions mediate the insertion of nanoparticles into model cell membranes. *Nat. Commun.* **5**, 4482 (2014).
23. R. C. Van Lehn, A. Alexander-Katz, Energy landscape for the insertion of amphiphilic nanoparticles into lipid membranes: A computational study. *PLoS One* **14**, e0209492 (2019).
24. S. Aeffner, T. Reusch, B. Weinhausen, T. Salditt, Energetics of stalk intermediates in membrane fusion are controlled by lipid composition. *Proc. Natl. Acad. Sci. U.S.A.* **109**, E1609–E1618 (2012).
25. M. E. Haque, B. R. Lentz, Roles of curvature and hydrophobic interstice energy in fusion: Studies of lipid perturbant effects. *Biochemistry* **43**, 3507–3517 (2004).
26. R. C. Van Lehn *et al*., Effect of particle diameter and surface composition on the spontaneous fusion of monolayer-protected gold nanoparticles with lipid bilayers. *Nano Lett.* **13**, 4060–4067 (2013).
27. R. C. Van Lehn, A. Alexander-Katz, Pathway for insertion of amphiphilic nanoparticles into defect-free lipid bilayers from atomistic molecular dynamics simulations. *Soft Matter* **11**, 3165–3175 (2015).
28. F. W. S. Stetter, L. Cwiklik, P. Jungwirth, T. Hugel, Single lipid extraction: The anchoring strength of cholesterol in liquid-ordered and liquid-disordered phases. *Biophys. J.* **107**, 1167–1175 (2014).
29. Y. Gao *et al*., Single reconstituted neuronal SNARE complexes zipper in three distinct stages. *Science* **337**, 1340–1343 (2012).
30. H. J. Risselada, H. Grubmüller, How SNARE molecules mediate membrane fusion: Recent insights from molecular simulations. *Curr. Opin. Struct. Biol.* **22**, 187–196 (2012).
31. D. Uhríková, N. Kučerka, J. Teixeira, V. Gordeliy, P. Balgavý, Structural changes in dipalmitoylphosphatidylcholine bilayer promoted by Ca2+ ions: A small-angle neutron scattering study. *Chem. Phys. Lipids* **155**, 80–89 (2008).
32. P. U. Atukorale *et al*., Structure-property relationships of amphiphilic nanoparticles that penetrate or fuse lipid membranes. *Bioconjug. Chem.* **29**, 1131–1140 (2018).
33. S. Trier, J. R. Henriksen, T. L. Andresen, Membrane fusion of pH-sensitive liposomes–A quantitative study using giant unilamellar vesicles. *Soft Matter* **7**, 9027–9034 (2011).
34. R. B. Lira, T. Robinson, R. Dimova, K. A. Riske, Highly efficient protein-free membrane fusion: A giant vesicle study. *Biophys. J.* **116**, 79–91 (2019).